CrossMark

Improved electrochemical performance of rGO/TiO$_2$ nanosheet composite based electrode for supercapacitor applications

Shashank Sundriyal[1,2] · Meenu Sharma[3] · Ashwinder Kaur[4] · Sunita Mishra[1,2] · Akash Deep[1,2]

Abstract

The present work reports the synthesis of a composite of TiO$_2$ nanosheets (NS) with reduced graphene oxide (rGO) for supercapacitor applications. The formation of composite has been achieved via a simple one-pot hydrothermal method. The rGO/TiO$_2$ NS composite was used to fabricate a flexible electrode which, in presence of 1 M H$_2$SO$_4$ as an electrolyte, has shown a high specific capacitance of 233.67 F/g at a current density of 1 A/g within a potential window of 0–1 V. This enhanced supercapacitance of the rGO/TiO$_2$ NS electrode is attributed to the synergistic effects from TiO$_2$ and rGO NS which help in to attain a low equivalent series resistance and enhanced ion diffusion. Furthermore, the fabricated composite electrode has displayed a long-term cyclic stability, retaining a specific capacitance of 98.2% even after 2000 charge–discharge cycles. The proposed rGO/TiO$_2$ NS electrode has delivered high values of energy (32.454 Wh/kg) and power (716.779 W/kg) densities. Interestingly, it is possible to retrieve a sufficiently high energy density of 24.576 Wh/kg which could generate a power density value of as high as 2142.84 W/kg. The above results reveal that the herein proposed thin film composite of rGO/TiO$_2$ NS can offer extraordinary performance as a supercapacitor electrode compared to its nanotubes or nanoparticles.

1 Introduction

A drastic depletion of fossil fuels along with the environmental issues associated with the use of conventional energy resources have intensified the demands for the development of alternative energy storage devices to produce clean and green energy. In this context, the supercapacitors have emerged as efficient electrochemical energy storage devices which help to bridge the gap between the electrolytic capacitors and batteries [1]. Due to the features of high specific capacitance, fast charging, high cyclic stability, and high power density with moderate energy density,

the supercapacitors find applications in hybrid electric vehicles, memory backup devices, and portable energy storage devices [2, 3]. They can be broadly classified into two categories: (i) electric double layer capacitors (EDLC), and (ii) pseudocapacitors [4–7]. The working mechanism of the EDLCs involves the storage of physical charge which results in an increased cyclic stability and good power density. Whereas, the pseudocapacitors are based on the faradaic redox reaction mechanism to realize high theoretical values of specific capacitance [8]. However, the specific capacitance of pseudocapacitors is drastically reduced when a high current density is to be drawn. Therefore, the recent research trends have advocated the development of devices which can hybridize the charge storage mechanism of both the EDLCs and pseudocapacitors [9–13].

Lately, graphene has been explored as a promising material for application in EDLCs. The use of graphene is associated with certain advantages such as high electrical conductivity and excellent chemical, thermal and mechanical stabilities [14, 15]. Amongst different functionalized forms of graphene, the reduced graphene oxide (rGO) with few defects offers better electrical conductivity than graphene oxide (GO) [16, 17]. As a limitation, the rGO nanosheets may suffer from the problem of agglomeration during their application in the formation of flexible electrodes [18]. This

✉ Sunita Mishra
  sunita_mishra@csio.res.in

✉ Akash Deep
  dr.akashdeep@csio.res.in

1 CSIR-Central Scientific Instrument Organisation (CSIR-CSIO), Chandigarh 160030, India

2 Academy of Scientific and Innovative Research (AcSIR-CSIO), Chandigarh 160030, India

3 Department of Physics, National Institute of Technology, Kurukshetra 136118, India

4 Department of Physics, Punjabi University, Patiala 147002, India

problem can negatively influence the conductivity, surface area and electrochemical performance of the fabricated electrodes. The incorporation of materials like conducting polymers, transition metal oxides (TMOs) and transition metal dichalcogenides (TMDs) between the rGO nanosheets has been reported to control their agglomeration [19, 20]. The use of TMOs like RuO_2, MnO_2, SnO_2, Fe_2O_3, TiO_2 and NiO have been proposed by many researchers to improve the specific capacitance of rGO based supercapacitor electrodes [21–28].

TiO_2 is projected as an attractive option for the preparation of composite electrodes in many charge storage devices due to its eco-friendliness, low production cost and excellent chemical stability [29, 30]. Recently, Xiang et al. has reported the hydrothermal fabrication of rGO/TiO_2 composite electrodes for supercapacitor applications. TiO_2 was used in the form of nanobelt (NB) and nanoparticle (NP). The fabricated electrodes displayed specific capacitances of 200 F/g (NB) and 60 F/g (NP) [31]. Lately, Sun et al. have also demonstrated the use of TiO_2 NP coated graphene sheets to attain a specific capacitance of 75 F/g [32]. However, this device had some limitations, e.g., low specific capacitance, poor cyclic stability, and requirements of high processing temperature and long reaction time. In another study, Ramadoss and Kim have reported the microwave assisted synthesis of graphene–TiO_2 hybrid structure which gave a specific capacitance value of 165 F/g [33]. Liu et al. have also investigated a GO/TiO_2 nanorod composite to attain a specific capacitance of 100 F/g [34]. Note that the above realized low levels of specific capacitances with the graphene–TiO_2 composites suggest the requirement of further research in this direction [35–37].

In the present research work, a simple one-pot hydrothermal method is reported to prepare a hybrid composite of rGO/TiO_2 nanosheets (rGO/TiO_2 NS). The sheet like morphology of the composite has facilitated the development of an efficient electrode for application in supercapacitors. As experimentally proven, rGO/TiO_2 NS electrode is characterized with beneficial properties of fast charge transport and high specific surface area. The achieved values of specific capacitance and energy density are better than the previously reported electrodes of similar materials.

2 Materials and methods

2.1 Materials

All the materials used in this study were of analytical/high purity grade and used without further purification. Amongst the major chemicals used during the research, graphite powder and titanium tetra-n-butoxide were purchased from Sigma Aldrich, India, while potassium permanganate ($KMnO_4$), hydrochloric acid (HCl), hydrofluoric acid (HF), sulfuric acid (H_2SO_4), hydrogen peroxide (H_2O_2), and sodium sulfate (Na_2SO_4) were purchased from Merck, India. Polyvinyldifluoridone (PVDF) and L-ascorbic acid were purchased from Himedia, India.

2.2 Synthesis of reduced graphene oxide (RGO)

First, graphene oxide (GO) was prepared from graphite powder as per an already reported method [16]. Briefly, graphite powder was mixed with $KMnO_4$ in a w/w ratio of 1:6 (1.5 g graphite and 9 g $KMnO_4$). Thereafter, this mixture was treated with an acidic reagent containing 180 mL of H_2SO_4 and 20 mL of H_3PO_4. The above action exothermically raised the temperature of the reaction mixture to about 35–40 °C. The temperature was then further raised up to 50 °C and the contents were left on continuous stirring for 2 h. Next, the reaction vessel was kept in an ice bath and allowed to get cooled to the room temperature. It was immediately followed by the addition of 1.5 mL of 30% H_2O_2. The reaction mixture was again stirred for about 30 min. Subsequently, it was centrifuged at 8000 rpm for 15 min to removes impurities like amorphous carbon and acidic content. More centrifugation steps (8000 rpm, 10 min) were provided (twice each with distilled water, 30% HCl and ethanol in that order) to wash and separate the desired product (GO). After drying at 80 °C, the product was manually crushed to form a fine powder before preserving it at room temperature conditions.

2.3 Synthesis of rGO/TiO_2 NS composite

As a first step in the formation of rGO/TiO_2 NS composite, 150 mg GO sample was ultrasonically dispersed in 50 mL of ethanol (3 h). Next, 3 mg/mL of ethanolic dispersion of GO was mixed and stirred (10 min) with 7 mL of titanium tetra-n-butoxide and 0.8 mL of HF. Subsequently, the reaction mixture was sealed in a Teflon lined stainless steel autoclave and heated to 180 °C for 24 h. After the reaction, the desired rGO/TiO_2 NS product was recovered by centrifugation (10,000 rpm, 15 min). It was washed with water (centrifugation step at 8000 rpm, 10 min), followed by drying under vacuum for 24 h. For some studies, pure TiO_2 nanosheets (i.e., reaction carried out in absence of rGO) were also prepared using the above procedure.

2.4 Material characterization

The XRD patterns were collected using a X-ray diffractometer (XRD, Bruker, D8 Advance Cu Kα λ = 1.54060 Å) over a 2θ range of 20°–70°. Raman spectra were recorded on a Renishaw (Invia) system by exciting the sample with a 532-nm laser source. The N_2 adsorption–desorption

measurements were carried out on a Belsorp Max system from Microtrac to calculate specific surface area and pore volume. Fourier transform infrared spectroscopy (FTIR) measurements were made by a FTIR spectrometer (Nicolet iS10) at a scan rate of 2.5 cm/s. The morphology and structural analysis of the samples were investigated with field emission scanning (FESEM, Hitachi S4800; applied voltage: 5–7 kV) and transmission (TEM, Technai G20; accelerating voltage: 200 kV) electron microscopes. The electrochemical measurements were carried out using a PGSTAT 302N instrument (Autolab, Metrohm).

2.5 Electrochemical measurements

The electrochemical measurements, e.g., cyclic voltammetry (CV), galvanostatic charge discharge (GCD) and electrochemical impedance spectroscopy (EIS), were recorded with a three-electrode system consisting of a platinum wire (Pt), Ag/AgCl, and the active material as counter, reference and working electrodes, respectively. The working electrode was prepared by mixing the active material, carbon black and polyvinyledene fluoride (PVDF) in a ratio (w/w) of 8:1:1. A uniform slurry of these components was prepared in *N*-methyl pyrrolidone solvent and then homogenously coated over a carbon paper (graffoil). The prepared electrode was dried in an oven (80 °C) for 12 h before use. The active mass ratio of the coated material over graffoil was 0.5 mg/cm^2.

1 M H_2SO_4 was used as the aqueous electrolyte in all the electrochemical studies. The CV measurements were obtained at various scan rates (20, 10, 5, 2, 1 mV/s) over a potential range of 0–1 V. The GCD measurements were also performed at various current densities (10, 5, 3, 2, 1 A/g) after setting the cut off potential at 1 V (vs. Ag/AgCl reference electrode). The EIS measurements were carried out over a frequency range of 0.1 Hz–100 KHz, maintaining an AC of amplitude of 10 mV.

3 Results and discussion

RGO/TiO$_2$ nanosheet composite has been prepared via a simple one-step hydrothermal process (schematic shown in Scheme 1). In the synthesis process, titanium tetra-*n*-butoxide is transformed into TiO$_2$ NS, which then decorate over GO NS. A subsequent thermal reduction step converts GO into rGO. The mechanism of the formation of TiO$_2$ NS during the hydrothermal processing of the precursors in an acidic medium has been explained in the literature [38]. Under such conditions, GO nanosheets also undergo quick deoxygenation to form rGO. Therefore, our approach has conveniently yielded the desired formation of rGO/TiO$_2$ NS composite.

3.1 Material characterizations

3.1.1 XRD studies

XRD patterns of the rGO NS (standard sample synthesized as per the earlier reported procedure [39]), TiO$_2$ NS (synthesized as detailed in Sect. 2.3), and rGO/TiO$_2$ NS composite (synthesized as detailed in Sect. 2.3) are shown in Fig. 1. The observed peak positions are in good agreement with

Scheme 1 Schematic for the synthesis for rGO/TiO$_2$ nano sheets
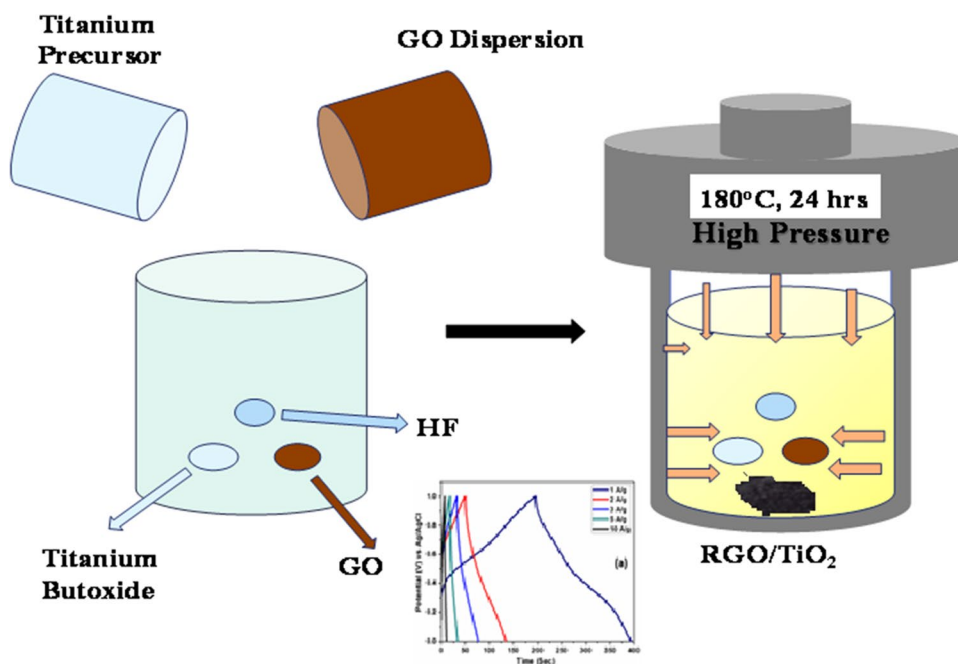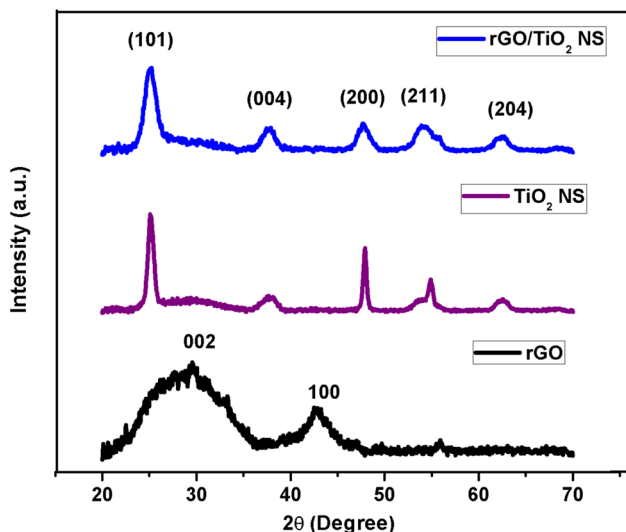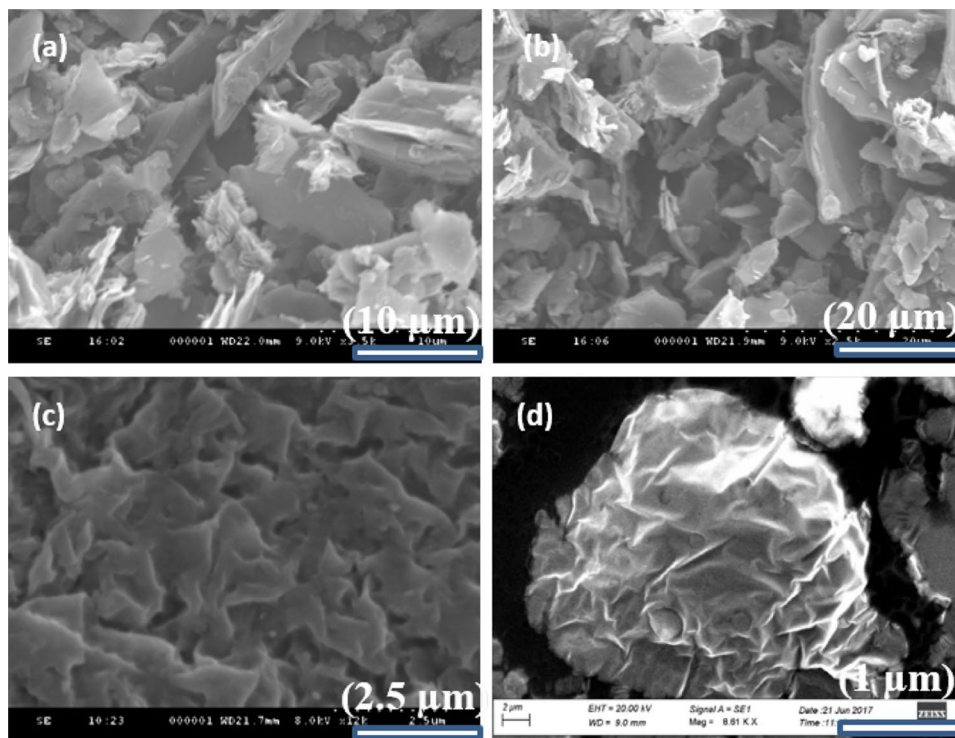
Fig. 1 XRD spectra of rGO/TiO$_2$ NS, TiO$_2$ NS and rGO samples

previous reports [38, 40, 41]. The (101) crystal plane peak at 25.2°, as observed in all the TiO$_2$ NS containing samples, indicates about the presence of titanium oxide in its anatase phase. All other well-defined diffraction peaks at 37.87°, 47.76°, 54.3° and 62.54° can also be assigned to the (004), (200), (211) and (204) reflections of crystalline planes of TiO$_2$ nanosheets (JCPDS No. 21-1272); indicative of the successful synthesis of TiO$_2$ NS in a single-step hydrothermal process [40].

An absence of GO specific reflections around 8°–10° suggest that all GO content was successfully reduced to rGO during the hydrothermal reaction [16, 41]. This was also validated by reflections at 27.67° and 42.5°, attributing to the (002) and (100) planes of rGO. As discussed in this section, the XRD studies have verified the formation of rGO/TiO$_2$ NS composite.

3.1.2 Morphological studies

FESEM images of the synthesized rGO, TiO$_2$ NS, and rGO/TiO$_2$ NS composite are shown in Fig. 2. Though the morphology of rGO and TiO$_2$ NS are almost similar, the latter sample is somewhat distinguishable with the appearance of folds and wrinkles. The morphological analysis also clearly shows the formation of rGO/TiO$_2$ NS composite in a 2-D sheet like pattern. The individual appearances of rGO and TiO$_2$ NS seem to have merged which indicates about the presence of both the components in the sample of rGO/TiO$_2$ NS. A morphological uniformity of the synthesized composite is vital for exploiting its application in the designing of electrodes for electronic devices, such as supercapacitors. It may also be noted that a crumpled morphology of the composite, mainly due to the presence of TiO$_2$ NS, should also facilitate fast transport of electrolyte ions over the electrode surface [42].

The TEM and high resolution TEM (HR-TEM) images of the samples also reveal a uniform and crumpled distribution of TiO$_2$ nanosheets over rGO sheets (Fig. 3). The HR-TEM

Fig. 2 FESEM investigations—**a, b** rGO, **c** TiO$_2$ NS, **d** rGO/TiO$_2$ NS composite

Fig. 3 TEM and HRTEM images of rGO/TiO$_2$ NS composite at different resolutions
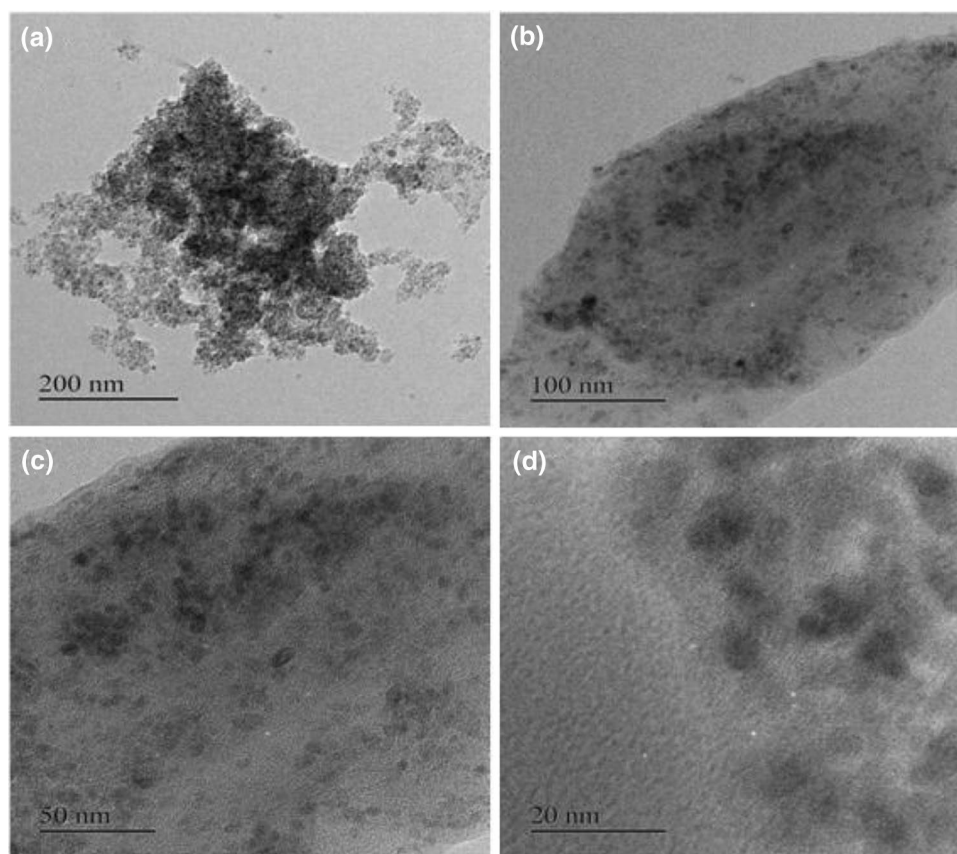
investigations characterize the crystalline TiO$_2$ NS with an interlayer distance of few nanometers. This is in good accordance with the (101) plane of anatase phase of TiO$_2$. Moreover, the edges of rGO sheets can also be very clearly observed. The above TEM investigations have highlighted the formation of a nanosheet like geometry of rGO/TiO$_2$ composite, which is beneficial for charge storage as well as the transport of electrolyte ions inside the porous network of electrode. These two important properties are highly useful for the realization of efficient supercapacitors.

3.1.3 Raman spectroscopy and FTIR studies

Raman spectroscopy has been used to study the vibrational modes of samples. The results of these analyses are shown in Fig. 4a. The rGO sample was characterized with two prominent peaks at 1357 and 1589 cm^{-1}, corresponding to the D and G bands. The D band is caused by the disorder and defects induced breathing mode of the sp^2 rings. This signal arises from the stretching of C–C bonds and is common to all carbon lattices that are sp^2 hybridised [33]. The G band results from the in-plane vibrations of sp^2 bonded carbon atoms. Its signal at 1589 cm^{-1} indicates about 1st order stretching of E$_{2g}$ phonon of sp^2 carbon atoms. A relatively higher intensity of the D band point outs to the formation of more sp^2 domains [43, 44].

rGO sample shows D to G bands (I$_D$/I$_G$) intensity ratio of 1.19 which is much larger than that for GO, implying the successful conversion of GO into rGO [16]. Raman spectrum for TiO$_2$ NS sample has shown the peaks for typical anatase phase, i.e., at 141, 386, 506 and 634 cm^{-1} corresponding to E$_g$, B$_{1g}$, A$_{1g}$ and E$_g$ vibrations, respectively [29, 38]. The rGO/TiO$_2$ NS sample shows collective peaks from both rGO (1346, 1588 cm^{-1}) and TiO$_2$ (141, 386, 506, 634 cm^{-1}) to confirm a successful formation of the desired composite material.

FTIR spectra of rGO, TiO$_2$ NS, and rGO/TiO$_2$ NS samples are shown in Fig. 4b. All the spectra show a common band around 3450 cm^{-1} to signify the surface O–H stretching vibrations of C–OH group. rGO sample shows band mainly corresponding to epoxide confirming a successful reduction of GO into rGO. The sample of TiO$_2$ NS displays a band around 556 cm^{-1} attributing to the presence of Ti–O stretching [45]. The analysis of rGO/TiO$_2$ NS shows a band around 1627 cm^{-1} which is associated to the skeletal vibration of rGO and depicts the presence of hydroxyl (–OH) and carbonyl (C=O) group in the formed composite. A rGO specific band around 1627 cm^{-1} indicates toward the formation of Ti–O–C bonds in the final NS composite.
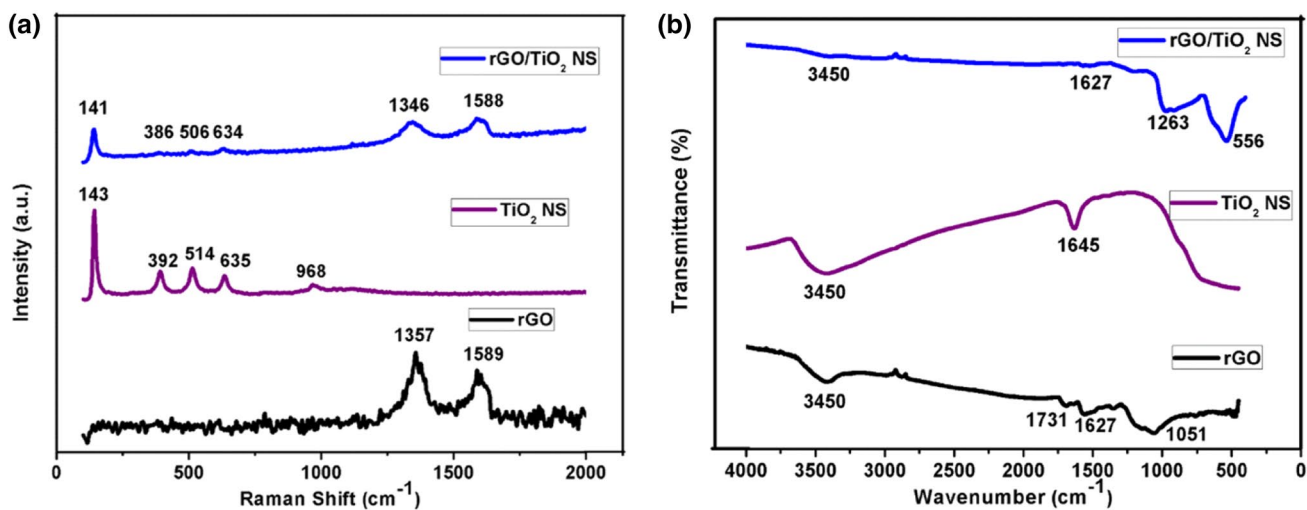
Fig. 4 a Raman spectra and **b** FTIR analysis of rGO, TiO_2 NS and rGO/TiO_2 NS samples

3.1.4 BET N_2 adsorption–desorption studies

The N_2 adsorption–desorption isotherms of rGO/TiO_2 NS composite and TiO_2 NS are shown in Fig. 5. In both the cases, typical type-IV sorption behavior with hysteresis loops suggests that the samples possess mesoporous structure [46]. The BET surface areas for the TiO_2 NS and rGO/TiO_2 NS samples are estimated as 119.6 and 213.6 m^2/g, respectively. The mesoporous nature of the samples is further confirmed by the Barrett Joyner Halenda (BJH) pore size distribution plots. The BJH analyses estimated the mean peak pore radius of pores in TiO_2 NS and rGO/TiO_2 NS to be as 2.49 and 1.96 nm, respectively. The N_2 adsorption–desorption study has highlighted the fact that the surface to volume ratio (i.e., the porosity) of the rGO/TiO_2 NS composite is largely improved compared to the TiO_2 nanosheets alone.

3.2 Electrochemical studies

3.2.1 Supercapacitor electrodes performance tests with cyclic voltammetry and galvanostatic charge discharge studies

CV and GCD measurements have been carried out to assess the specific capacitance, energy density and power density of the fabricated electrodes. The CV measurements for TiO_2 NS and rGO/TiO_2 NS working electrodes at various scan rates (20, 10, 5, 2 and 1 mV/s) are shown in Fig. 6. In these experiments, the working voltage was 1 V and the parameters were recorded in a potential range of 0–1 V using 1 M H_2SO_4 as an aqueous electrolyte. The CV analysis of TiO_2 NS shows anodic and cathodic redox peaks attributing to the pseudocapacitive nature of the sample. In the case of rGO/TiO_2 NS too, these peaks were discernible even at low scan

rates, thereby confirming the co-presence of TiO_2 NS. Further, in addition to pseudocapacitive property the involvement of rGO facilitates EDLC characteristics in the hybrid composite. As CV curves depict, the specific capacitance of the system was found to decline as scan rate increased from 1 to 20 mV/s. This may be accounted for by the fact that higher scan rates may not provide sufficient time for the electrolyte ions to be subjected to adsorption/desorption at the electrode interface.

CV data have been utilized to calculate the values of specific capacitances (C_s, in F/g) for different fabricated electrodes using the following equation [47]:

$$Cs = \frac{\int IdV}{ms\Delta V} \tag{1}$$

where ($\int IdV$) is the integral area of CV curve, m is the mass of active material on the electrode in g, s is the scan rate in mV/s, and ΔV is the total potential deviation of the voltage window.

The values of specific capacitance for rGO/TiO_2 nanosheet electrode have been estimated as 228.27 and 146.86 F/g at scan rates of 1 and 5 mV/s, respectively.

GCD measurements are known to offer a reliable method of assessing the specific capacitance of supercapacitors electrodes at a constant current density (chrono-potentiometry mode). Figure 7 shows GCD curves for our TiO_2 NS and rGO/TiO_2 NS electrodes at different current densities, i.e. 10, 5, 3, 2, and 1 A/g. All the GCD plots shows non-linear curves (nearly triangular shape) which is attributed to the formation of rGO (EDLC characteristic) and TiO_2 NS (pseudocapacitive characteristic) hybrid [11, 48]. The observed profiles exhibit only a small voltage drop to indicate a low internal resistance of the electrodes. A comparison between the different electrodes clearly suggests towards a higher
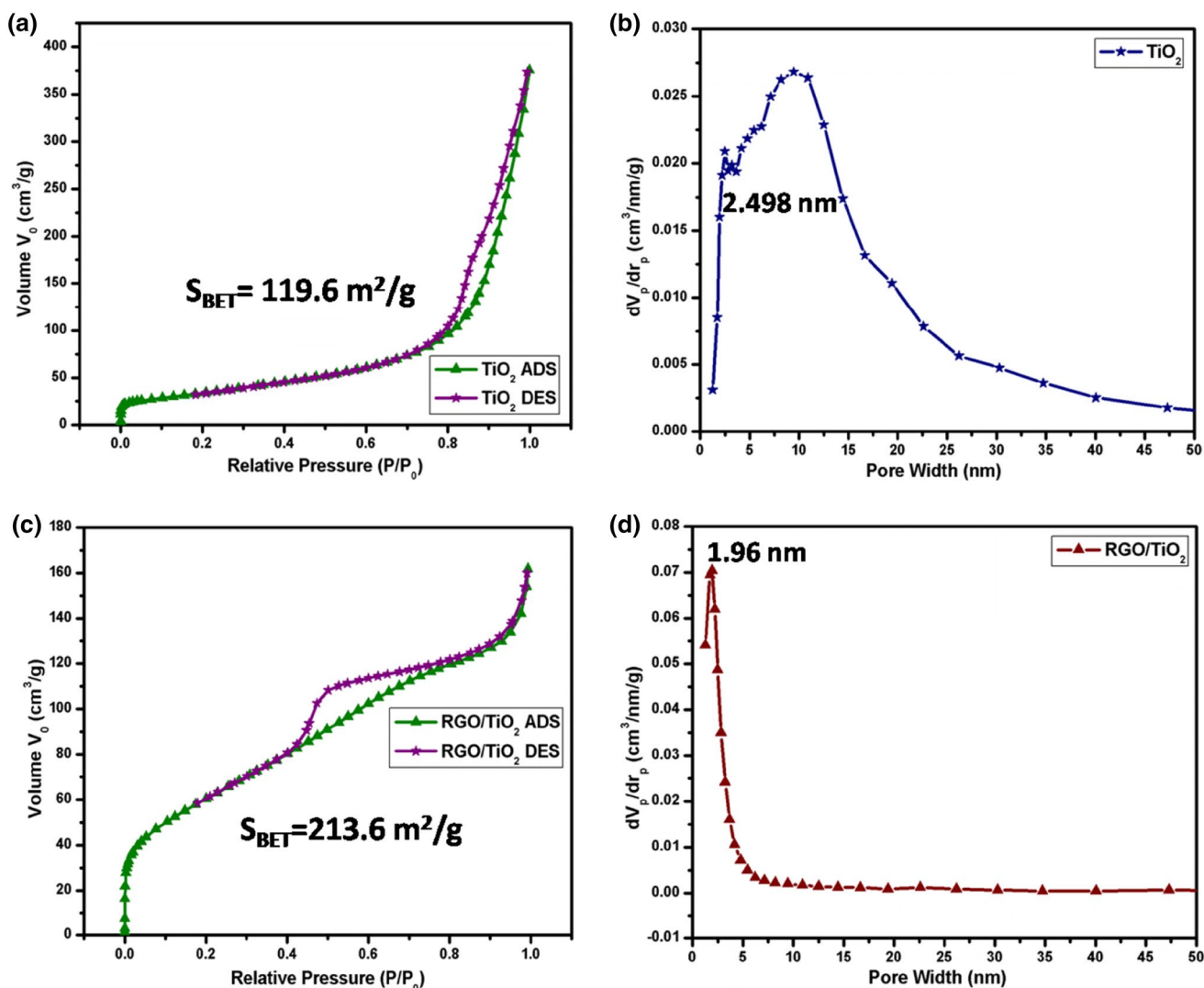
Fig. 5 **a, c** N$_2$ adsorption–desorption isotherms for TiO$_2$ NS and rGO/TiO$_2$ NS, respectively; **b, d** BJH pore size distribution plots for TiO$_2$ and rGO/TiO$_2$ NS, respectively

electronic conductivity and a better charge transport rate obtained with the use of rGO/TiO$_2$ NS composite. GCD plots also reveal about decreasing discharging time with the increasing current density, or vice versa (Fig. 8b). This behavior can be explained by the reduced chances of a complete diffusion of electrolyte ions into the pores of the electrode material at higher current densities [49].

Using the GCD data, the specific capacitances (Cs) of the electrodes have been calculated according to the following equation [48]:

$$Cs = \frac{I\Delta t}{m\Delta V} \qquad (2)$$

where Δt is the discharge time, m is the mass of active materials on the electrode in g, ΔV is the total potential deviation of the voltage window.

The highest values of specific capacitance for TiO$_2$ NS and rGO/TiO$_2$ NS electrodes have been estimated as 133.1 and 233.67 F/g, respectively at a current density of 1 A/g. The value obtained for the herein developed rGO/TiO$_2$ NS composite electrode is much higher than that reported previously with the use of rGO/TiO$_2$ NS composites prepared in the geometries of nanoparticles [31], nanotubes [50], nanobelts [31], and nanofibers [46] (Table 1). The improved performance of our rGO/TiO$_2$ NS composite can be attributed to nanosheet type morphology of the electrode material which bears a higher surface to volume ratio and allows better charge transport.

We have also investigated the cyclic stability of our rGO/TiO$_2$ NS electrode for 2000 cycles. As shown in Fig. 8c, almost 98.2% of the electrode capacity could be retained after performing 2000 continuous charge–discharge cycles.
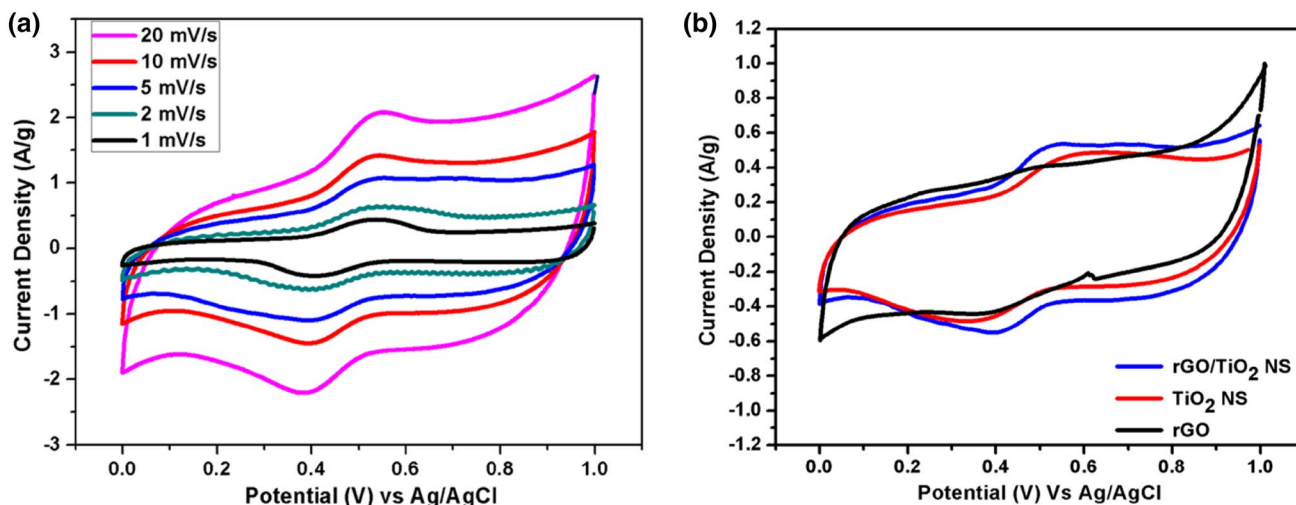
Fig. 6 **a** CV curves recorded for rGO/TiO$_2$ NS composite electrode at different scan rates; **b** comparative CV curves for rGO, TiO$_2$ NS and rGO/TiO$_2$ NS electrodes at a scan rate of 5 mV/s
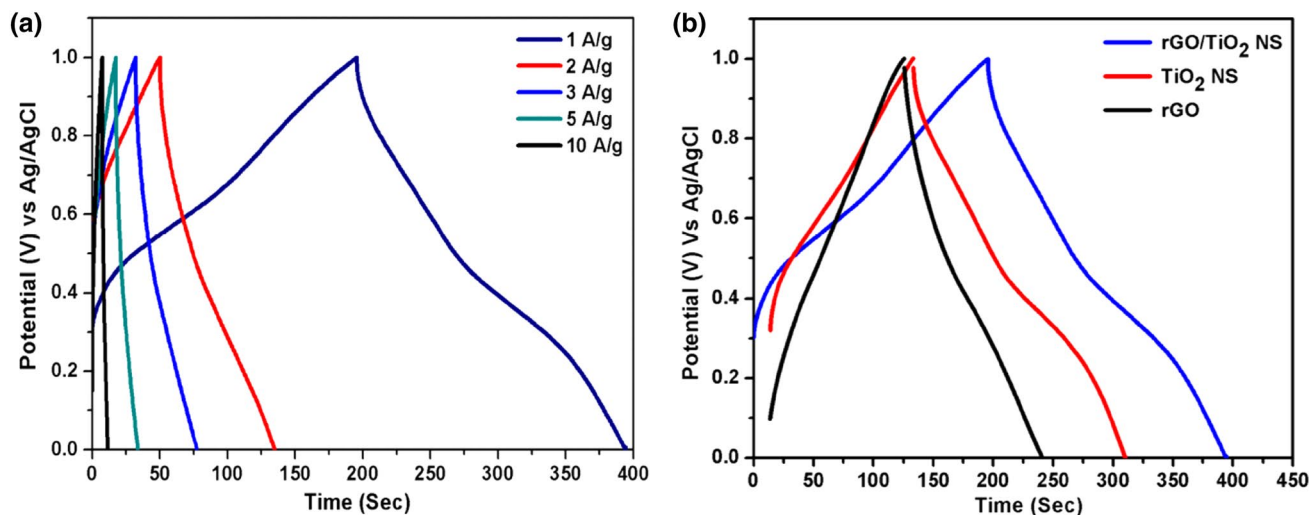

Fig. 7 **a** GCD plots for rGO/TiO$_2$ NS at different current densities; **b** comparative GCD plots for rGO, TiO$_2$ NS and rGO/TiO$_2$ NS at a current density of 1 A/g

The energy (Es) and power (Ps) densities are two important parameters to assess the overall electrochemical performance of any supercapacitor electrode. These parameters for the fabricated electrodes have also been computed as per the following expressions:

$$Es = \frac{Cs\Delta V^2}{7.2} \tag{3}$$

$$Ps = \frac{3600 Es}{\Delta t} \tag{4}$$

where Cs is the specific capacitance in F/g, ΔV is the total potential deviation of the voltage window, and Δt is the discharge time

RGO/TiO$_2$ nanosheet electrode has delivered very good values of energy and power densities as 32.454 Wh/kg and 716.779 W/kg, respectively (Fig. 8d). Using this electrode, it is also possible to withdraw a power density of as high as 2142.84 W/kg wherein the value of energy density was 24.576 Wh/kg. These values highlight about the extraordinary performance and stability of the proposed rGO/TiO$_2$ nanosheets electrode. A combination of EDLC and faradaic capacitance, achieved by the double layer charging process, leads to a non-faradaic charge transfer mechanism.
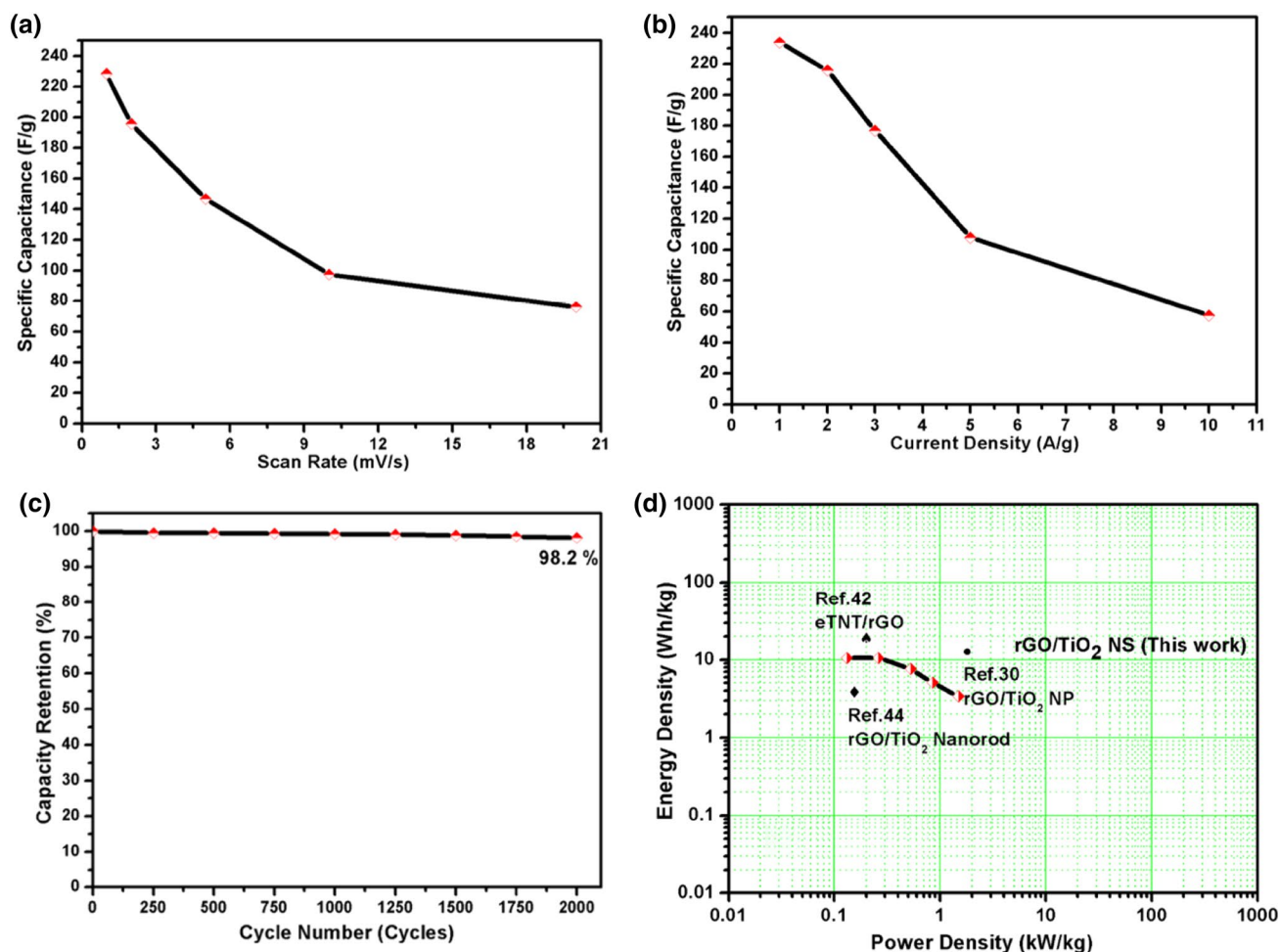
Fig. 8 **a** Variation in the specific capacitance values of rGO/TiO$_2$ NS electrode with respect to the scan rate; **b** variation in the specific capacitance values of rGO/TiO$_2$ NS electrode with respect to the current density; **c** cyclic stability of rGO/TiO$_2$ NS electrode at a current density of 10 A/g; **d** Ragone plot for rGO/TiO$_2$ NS electrode

Table 1 A comparison of supercapacitor performance of rGO/TiO$_2$ NS electrode with earlier reported graphene/TiO$_2$ electrodes

| S. no.	Electrode material	Electrolyte	Scan rate/current density	Specific capaci-tance (F/g)	Energy den-sity (Wh/Kg)	Capacitance reten-tion % (w.r.t cyclic stability)	Ref.
1	Graphene/TiO$_2$ NPs hybrid	1 M Na$_2$SO$_4$	5 mV/s	165	12.5	90 (5000 cycles)	[33]
2	rGO/TiO$_2$ nanobelts	1 M Na$_2$SO$_4$	2 mV/s (0.125 A/g)	200 (225)	20.1	86.5 (2000 cycles)	[31]
3	rGO/TiO$_2$ NPs	1 M Na$_2$SO$_4$	2 mV/s (0.125 A/g)	60 (62.8)	8.3	–	[31]
4	eTNT/rGO	1 M Na$_2$SO$_4$	1 A/g	165.6	16.5	93.3 (3000 cycles)	[50]
5	rGO/TiO$_2$ nanorod	1 M Na$_2$SO$_4$	5 mV/s	114.5	6.30	85 (4000 cycles)	[51]
6	TiO$_2$/graphene	1 M KOH	10 mV/s	84	–	87.5 (1000 cycles)	[32]
7	GO/TiO$_2$ nanorod	1 M Na$_2$SO$_4$	5 mV/s	100	–	80 (3000 cycles)	[34]
8	rGO/TiO$_2$ nanofibers aerogels	1 M Na$_2$SO$_4$	1 A/g	178	–	90.4 (3000 cycles)	[46]
9	TiO$_2$/graphene hydrogel	0.5 M Na$_2$SO$_4$	0.5 A/g	206	–	96.4 (2000 cycles)	[52]
10	Co doped TiO$_2$/rGO com-posites	0.5 M Na$_2$SO$_4$	5 mV/s	34.8	0.95	–	[53]
11	rGO/TiO$_2$ NS	1 M H$_2$SO$_4$	1 A/g	233.67	32.454	98.2 (2000 cycles)	This work
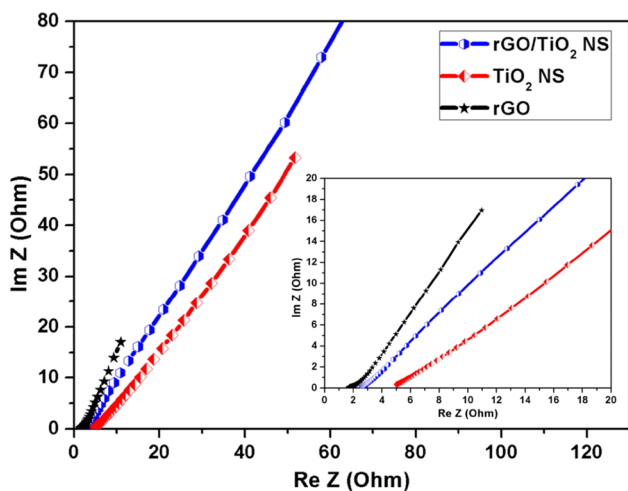
Fig. 9 Nyquist plot recorded for rGO, TiO_2 NS and rGO/TiO_2 NS electrodes (inset showing magnified Nyquist plot of all three electrodes)

Therefore, the device also takes a long time for discharging which is an added benefit.

To the best of the authors' knowledge, the herein developed rGO/TiO_2 NS electrode offers superior values of specific capacitance and energy density than most of the previously reported composites of the same materials (Table 1). The electrode also displays a better cyclic stability.

3.2.2 Electrochemical impedance spectroscopy studies

Electrochemical impedance spectroscopy (EIS) measurements also allow the assessment of an electrode's performance in supercapacitor applications. Nyquist plot, derived from the EIS data, is used to determine the values for various impedance parameters, namely series resistance (R_s), charge transfer resistance (R_{ct}), Electric double layer (EDL) capacitance, and Warburg resistance (W or R_w). The EIS characteristics of our TiO_2 NS and rGO/TiO_2 NS electrodes are depicted in Fig. 9. These analyses were carried out at room temperature conditions using the frequency response analyzer (FRA) module of the system's software. The Nyquist plots drawn for all the three materials, i.e. rGO, TiO_2 NS and rGO/TiO_2 NS, were almost similar in shape. Generally, the Nyquist plots with semicircular shape are associated with the R_{ct} component, while inclined line is attributed to the Warburg impedance [5, 26]. In our results, the semicircle shape was somehow attenuated in all the cases indicating that the ion diffusion/transport at the electrode/electrolyte interface was largely dependent upon the applied frequency.

The values of the equivalent series resistance (ESR) are calculated to be 1.67, 4.9 and 2.83 Ω for rGO, TiO_2 NS and rGO/TiO_2 NS electrodes, respectively. The values of R_{ct} calculated for these electrodes are very low (in the range

of 0.62, 0.85 and 0.71 Ω), as also visually testified from the appearances of small semicircles in all the cases. The low values of ESR and R_{ct} may be attributed to the dispersion of TiO_2 NS in the composite which prevented restacking of rGO NS. It may also be noted that the low R_{ct} value are an indication of good electrochemical performance. These low R_{ct} values agree well with the already discussed GCD observations which also show a very low degree of the voltage drop. Thus, the present studies have proven that a nanosheet like morphology of the rGO/TiO_2 NS composite provides an efficient electron transport across the electrolyte/electrode interface. All the above favoring aspects ensure an efficient design of an electrode with high electrical conductivity.

4 Conclusions

The present research has demonstrated the application of rGO/TiO_2 NS composite electrode for achieving enhanced supercapacitor performance. The composite has been prepared by an easy one-step hydrothermal process. The synergistic effects between rGO and TiO_2 NS have resulted in improved electrochemical performance in terms of specific capacitance and cyclic stability than the previously reported graphene/TiO_2 electrode systems. These results have been achieved by using 1 M H_2SO_4 as an aqueous electrolyte while operating the system within a potential window of 1 V. RGO/TiO_2 NS electrode has exhibited a specific capacitance of 233.67 F/g at a current density of 1 A/g. An excellent cyclic stability of 98.2% has been achieved even after performing 2000 steps of charging-discharging. The improved electrochemical performance of rGO/TiO_2 NS composite can be attributed to the sheet like morphology of TiO_2 nanosheets crumpled within the rGO nanosheets. From the best of our knowledge, the herein proposed design of the rGO/TiO_2 NS electrode has offered a much better degree of cyclic stability (98.2%) and improved energy density (32.454 Wh/kg) than the earlier documented electrodes of the same material.

References

1. P.G. Bruce, S.A. Freunberger, L.J. Hardwick, J.-M. Tarascon, Nat. Mater. **11**, 19 (2012)
2. R. Ramachandran, S.-M. Chen, G.G. Kumar, Int. J. Electrochem. Sci. **10**, 10355 (2015)
3. N. Devillers, S. Jemei, M.-C. Péra, D. Bienaimé, F. Gustin, J. Power Sources **246**, 596 (2014)

4. T. Brousse, D. Bélanger, J.W. Long, J. Electrochem. Soc. **162**, A5185 (2015)
5. P.J. Hall, M. Mirzaeian, S.I. Fletcher et al., Energy Environ. Sci. **3**, 1238 (2010)
6. H. Jiang, L. Yang, C. Li, C. Yan, P.S. Lee, J. Ma, Energy Environ. Sci. **4**, 1813 (2011)
7. P. Simon, T. Brousse, F. Favier, *Supercapacitors Based on Carbon or Pseudocapacitive Materials* (Wiley, Hoboken, 2017), p. 39
8. L.L. Zhang, X. Zhao, Chem. Soc. Rev. **38**, 2520 (2009)
9. J.-M. Tarascon, M. Armand, Nature **414**, 359 (2001)
10. P. Simon, Y. Gogotsi, Nat. Mater. **7**, 845 (2008)
11. B.E. Conway (2013) *Electrochemical Supercapacitors: Scientific Fundamentals and Technological Applications* (Springer, New York, 2013)
12. G. Wang, L. Zhang, J. Zhang, Chem. Soc. Rev. **41**, 797 (2012)
13. S. Sundriyal, H. Kaur, S.K. Bhardwaj, S. Mishra, K.-H. Kim, A. Deep, Coord. Chem. Rev. **369**, 15 (2018)
14. K.S. Novoselov, A. Geim, Nat. Mater. **6**, 183 (2007)
15. P. Simon, T. Brousse, F. Favier, (2017) *Supercapacitors Based on Carbon or Pseudocapacitive Materials* (Wiley, Hoboken, 2017) p. 1
16. D.C. Marcano, D.V. Kosynkin, J.M. Berlin et al., ACS Nano **4**, 4806–4814 (2010)
17. W. Humers, R. Offeman, J. Am. Chem. Soc. **80**, 1339 (1958)
18. K.S. Novoselov, A.K. Geim, S.V. Morozov et al., Science **306**, 666 (2004)
19. Y. Wang, Z. Shi, Y. Huang et al., J. Phys. Chem. C **113**, 13103 (2009)
20. Y. Huang, J. Liang, Y. Chen, Small **8**, 1805 (2012)
21. J. Yan, Z. Fan, T. Wei, W. Qian, M. Zhang, F. Wei, Carbon **48**, 3825 (2010)
22. J.W. Lee, A.S. Hall, J.-D. Kim, T.E. Mallouk, Chem. Mater. **24**, 1158 (2012)
23. C. Lokhande, D. Dubal, O.-S. Joo, Curr. Appl. Phys. **11**, 255 (2011)
24. Y. Wang, C.Y. Foo, T.K. Hoo, M. Ng, J. Lin, Chem.-Eur. J. **16**, 3598 (2010)
25. D.P. Dubal, R. Holze, J. Power Sources **238**, 274 (2013)
26. D.P. Dubal, J.G. Kim, Y. Kim, R. Holze, W.B. Kim, Energy Technol. **1**, 125 (2013)
27. G.S. Gund, D.P. Dubal, B.H. Patil, S.S. Shinde, C.D. Lokhande, Electrochim. Acta **92**, 205 (2013)
28. U. Patil, R. Salunkhe, K. Gurav, C. Lokhande, Appl. Surf. Sci. **255**, 2603 (2008)
29. M. Salari, S.H. Aboutalebi, K. Konstantinov, H.K. Liu, Phys. Chem. Chem. Phys. **13**, 5038 (2011)
30. J. Shen, B. Yan, M. Shi, H. Ma, N. Li, M. Ye, J. Mater. Chem. **21**, 3415 (2011)
31. C. Xiang, M. Li, M. Zhi, A. Manivannan, N. Wu, J. Mater. Chem. **22**, 19161 (2012)
32. X. Sun, M. Xie, G. Wang et al., J. Electrochem. Soc. **159**, A364 (2012)
33. A. Ramadoss, S.J. Kim, Carbon **63**, 434 (2013)
34. R. Liu, W. Guo, B. Sun, J. Pang, M. Pei, G. Zhou, Electrochim. Acta **156**, 274 (2015)
35. N. Ahmadi, A. Nemati, M. Bagherzadeh, J. Alloys Compd. (2018). https://doi.org/10.1016/j.jallcom.2018.01.105
36. B. Endrődi, E. Kecsenovity, K. Rajeshwar, C. Janáky, ACS Appl. Energy Mater. **1**, 851 (2018)
37. P.A.K. Reddy, C. Manvitha, R. Boddula, S. Vattikuti, M.K. Kumar, C. Byon, Mater. Res. Bull. **98**, 314 (2018)
38. W. Wang, Z. Wang, J. Liu et al., Sci. Rep. **7** (2017)
39. J. Zhang, H. Yang, G. Shen, P. Cheng, J. Zhang, S. Guo, Chem. Commun. **46**, 1112 (2010). https://doi.org/10.1039/B917705A
40. Y. Zhang, N. Zhang, Z.-R. Tang, Y.-J. Xu, Phys. Chem. Chem. Phys. **14**, 9167 (2012)
41. H.M. Hassan, V. Abdelsayed, S.K. Abd El Rahman et al., J. Mater. Chem. **19**, 3832 (2009)
42. R. Bolagam, R. Boddula, P. Srinivasan, J. Solid State Electrochem. (2017). https://doi.org/10.1007/s10008-016-3487-x
43. K.N. Kudin, B. Ozbas, H.C. Schniepp, R.K. Prud'Homme, I.A. Aksay, R. Car, Nano Lett. **8**, 36 (2008)
44. T. Jawhari, A. Roid, J. Casado, Carbon **33**, 1561 (1995)
45. S. Stankovich, D.A. Dikin, R.D. Piner et al., Carbon **45**, 1558 (2007)
46. T.-W. Kim, S.-J. Park, J. Colloid Interface Sci. **486**, 287 (2017)
47. A. Ghosh, Y.H. Lee, ChemSusChem **5**, 480 (2012)
48. Y. Zhu, S. Murali, M.D. Stoller et al., Science **332**, 1537 (2011)
49. J.R. Miller, A.F. Burke, Electrochem. Soc. Interface **17**, 53 (2008)
50. Y. Zhang, F. Wang, H. Zhu, D. Zhang, J. Chen, Compos. A **101**, 297 (2017)
51. A. Ramadoss, G.-S. Kim, S.J. Kim, CrystEngComm **15**, 10222 (2013)
52. Z. Zhang, F. Xiao, Y. Guo, S. Wang, Y. Liu, ACS Appl. Mater. Interfaces **5**, 2227 (2013)
53. H. Xiao, W. Guo, B. Sun, M. Pei, G. Zhou, Electrochim. Acta **190**, 104 (2016)